1 Full Title: High affinity Na^+ transport by wheat HKT1;5 is blocked by K^+

2

3 Running title: HKT1;5 proteins catalyse dual affinity Na^+ transporter in wheat

4 Authors: Bo Xu[1,2], Maria Hrmova[2] and Matthew Gilliham[1,2*]

5

6 [1]Australian Research Council Centre of Excellence in Plant Energy Biology,
7 University of Adelaide, Waite Research Precinct, Glen Osmond, South Australia
8 5064, Australia

9

10 [2]School of Agriculture, Food and Wine, and Waite Research Institute, University of
11 Adelaide, Waite Research Precinct, Glen Osmond, South Australia 5064, Australia

12

13 [*]Corresponding author: e-mail: matthew.gilliham@adelaide.edu.au

14

15

16

17

Abstract

The wheat sodium transporters TmHKT1;5-A and TaHKT1;5-D are encoded by genes underlying major shoot Na^+ exclusion loci *Nax2* and *Kna1* from *Triticum monococcum* (Tm) and *Triticum aestivum* (Ta), respectively. In contrast to HKT2 transporters that have been shown to exhibit high affinity K^+-dependent Na^+ transport, HKT1 proteins have, with one exception, only been shown to catalyse low affinity Na^+ transport and no K^+ transport. Here, using heterologous expression in *Xenopus laevis* oocytes we show that both TmHKT1;5-A and TaHKT1;5-D encode dual (high and low) affinity Na^+-transporters with the high-affinity component being abolished when external K^+ is in excess of external Na^+. The low-affinity component for Na^+ transport of TmHKT1;5-A had a lower K_m than that of TaHKT1;5-D even when blocked by external K^+. We use 3-D structural modelling to explain how K^+ block may occur and propose potential physiological consequences of K^+ block. The transport properties and localisation of wheat HKT1;5 proteins are well suited for their role in a 'gatekeeper' process that secure shoot Na^+-exclusion and underpin recent advances for improving crop plant salt tolerance.

Keywords: salinity; High-affinity K Transporters; HKT; wheat; membrane transport; crop; 3-D structural modelling

38 **Introduction**

39 Crops suffer reduced growth and productivity under salinity stress. Salt, when it
40 builds up to high concentrations in the growing medium (i.e. soil solution) imposes an
41 osmotic limitation on water uptake, interferes with optimal nutrient homeostasis, and
42 leads to the build up of leaf cellular sodium (Na^+) concentrations, which causes an
43 ionic toxicity that limits photosynthesis and carbon assimilation in plants (Munns and
44 Gilliham, 2015).

45

46 A major genetic mechanism contributing towards salinity tolerance of most crops
47 including the cereals rice (*Oryza sativa*) and wheat (*Triticum aestivum* and *Triticum*
48 *monococcum*) is Na^+ exclusion from leaves, with the High-affinity potassium (K^+)
49 transporter (HKT) protein family having a major role in this trait (Ren *et al.* 2005;
50 James *et al.* 2006; Munns *et al.* 2012; Munns and Gilliham, 2015; Campbell *et al.*
51 2017; Xu *et al.* 2018). This family of proteins are represented widely across the plant
52 kingdom, and more broadly are members of the high affinity K^+/Na^+ transporting
53 Ktr/TrK/HKT superfamily of proteins that are present in bacteria (Ktr and TrK), fungi
54 (TrK) and plants (HKT) (Sentenac and Bonneaud 1992; Corratgé-Faillie *et al.* 2010).

55

56 These plant HKTs are divided into 2 clades: 1) class 1 HKT proteins (HKT1;x) are
57 mostly Na^{+-}selective transporters; 2) whereas class 2 HKTs (HKT2;y) mostly function
58 as K^+-Na^+ symporters and so far have been only identified in cereal monocots (Asins
59 *et al.* 2013; Waters *et al.* 2013). This definition has been challenged on occasion, such
60 as for OsHKT2;4 following its characterization in *Xenopus laevis* oocytes, where
61 there are conflicting reports on its permeability to Ca^{2+}, Mg^{2+} and NH_4^+ in addition to
62 K^+ and Na^+ (Lan *et al.* 2010; Horie *et al.* 2011; Sassi *et al.* 2012). Furthermore, there
63 are two reports of K^+ permeability in the HKT1 clade . Firstly, Arabidopsis AtHKT1
64 could complement K^+ transport deficient *E. coli* although no K^+ permeability could be
65 found when it was expressed in *X. laevis* oocytes in the same study (Uozumi *et al.*,
66 2000). Secondly, *Eucalyptus camaldulensis* EcHKT1;1 and EcHKT1;2, which appear
67 to be the exception for the HKT1 proteins characterized so far in that as they transport
68 both Na^+ and K^+ when expressed in *X. laevis* oocytes (Liu *et al.* 2001). Other HKT1
69 transporters have no reported K^+ permeability (Uozumi *et al.* 2000; Mäser *et al.* 2002;
70 Platten *et al.* 2006; Jabnoune *et al.* 2009; Cotsaftis *et al.* 2012; Munns *et al.* 2012;
71 Waters *et al.* 2013; Byrt *et al.* 2014; Campbell *et al.* 2017; Henderson et al., 2018).

72

73 Whilst K^+ transport is not a common feature of HKT1 transporters, several have
74 shown the property of K^+-regulated Na^+ transport (Ben Amar *et al.* 2013; Almeida *et*
75 *al.* 2014a; Almeida *et al.* 2014b; Byrt *et al.* 2014). For instance, the presence of 10
76 mM external K^+ ($[K^+]_{ext}$) reduced the inward Na^+ current of *X. laevis* oocytes
77 expressing *HKT1;5* from *T. aestivum* (*TaHKT1;5-D*) at -140 mV (Byrt *et al.* 2014),
78 and the outward Na^+ current of that expressing *HKT1;2* from *Solanum lycopersicum*
79 (*SlHKT1;2*) (Almeida *et al.* 2014a). Interestingly, $[K^+]_{ext}$ stimulated both inward and
80 outward Na^+ transport of *X. laevis* oocytes expressing two *HKT1;4* alleles from
81 *Triticum turgidum* L. subsp. *durum* when assayed with solutions of very low ionic
82 strength (Ben Amar *et al.* 2013).
83
84 Ktr/TrK/HKT proteins are predicted to consist of 8 transmembrane domains that fold
85 into 4 pseudo-tetramers around a central pore (Mäser *et al.*, 2002; Cotsaftis *et al.*,
86 2012; Xu *et al.*, 2018). The selectivity filter lining the pore of Ktr and TrK and class 2
87 HKT proteins is predicted to be composed of four glycine residues. In class 1 HKTs
88 the first glycine within the predicted selectivity filter is substituted with a serine
89 (Mäser *et al.*, 2002); the lack of K^+ permeability in this clade has been linked to the
90 presence of this glycine (Uozumi *et al.*, 2000; Mäser *et al.*, 2002; Platten *et al.*, 2006;
91 Cotsaftis *et al.*, 2012; Waters *et al.*, 2013); but the exact mechanism underlying this
92 block is to be determined.
93
94 Here, we further characterise HKT1;5 proteins underlying two major salt tolerance
95 associated loci, *TmHKT1;5-A* (*Nax2*) and *TaHKT1;5-D* (*Kna1)* from *T. monococcum*
96 *and T. aestivum* respectively. We find that both TmHKT1;5-A and TaHKT1;5-D
97 encode dual affinity Na^+-transporters and that their dual affinity Na^+ transport can be
98 blocked by raising external K^+ concentration, and we propose the residues within the
99 selectivity filter that cause this block. This is the first report that Na^+ transport has two
100 affinities in the HKT1 clade and demonstrates that dual affinity transport is a common
101 property of both clades of the HKT family.
102
103
104
105

106 **Results**

107 **K^+ sensitivity of TmHTK1;5-A and TaHKT1;5-D**

108 Previously, it was shown that inward Na^+ transport for both TmHKT1;5-A and
109 TaHKT1;5-D was inhibited by external K^+ (Munns *et al.* 2012; Byrt *et al.* 2014).
110 Here, we further compared the K^+-sensitivity of between TmHKT1;5-A and
111 TaHKT1;5-D (Fig. 1). An increase in $[K^+]_{ext}$ to 30 mM reduced the channel
112 conductance of TmHKT1;5-A at -140 mV by approximately 75% in a 1 mM Na^+
113 ($[Na^+]_{ext}$) bath solution; similarly this amount of K^+ inhibited that of TaHKT1;5-D up
114 to 95 % (Fig. 1A, B and Fig. 2). However, such Na^+-inhibition by K^+ was gradually
115 decreased by increasing $[Na^+]_{ext}$ (Fig 1 and 2). For instance, 10 mM $[K^+]_{ext}$ suppressed
116 the channel conductance of TmHKT1;5-A by 43.5% in 1 mM $[Na^+]_{ext}$ and by 16.5%
117 in 10 mM $[Na^+]_{ext}$; it similarly reduced the TaHKT1;5-D conductance by 57% in 1
118 mM $[Na^+]_{ext}$ and by 23% in 10 mM $[Na^+]_{ext}$ (Fig. 1 and 2). When $[Na^+]_{ext}$ was
119 increased to 30 mM, the channel conductance of TmHKT1;5-A was insensitive to
120 $[K^+]_{ext}$, whereas that of TaHKT1;5-D was still inhibited (Fig. 2).
121
122 The increase in $[K^+]_{ext}$ from 0 to 10 mM did not significantly change the reversal
123 potential of TmHKT1;5-A or TaHKT1;5-D; all reversal potentials were close to the
124 theoretical equilibrium potential for Na^+ under all conditions (Fig. 3A,B). Moreover,
125 the observed shift in reversal potential was close to the theoretical Nernst shift for Na^+
126 regardless of the presence or absence of 10 mM $[K^+]_{ext}$ (Fig. 3). This suggests that
127 neither of protein were permeable to K^+.
128

129 **Dual affinity transport of Na^+ by TmHTK1;5-A and TaHKT1;5-D**

130 The affinity for Na^+ transport of TmHKT1;5-A was previously reported to be ~4-fold
131 higher than the Na^+-transport affinity of TaHKT1;5-D (Munns *et al.* 2012; Byrt *et al.*
132 2014; Xu *et al.* 2018), which we confirm here (Fig. 4A,B). On closer examination, we
133 found a property that has not been described before. When lower concentrations of
134 $[Na^+]_{ext}$ were present it was clear that the concentration dependence of inward Na^+
135 currents could be fitted by two components, for both TmHKT1;5-A and TaHKT1;5-D
136 (Fig. 4). Whilst both components were saturable, the concentration at which both
137 phases saturated were greater for TaHKT1;5-D compared to TmHKT1;5-A (Fig.
138 4A,B). For TmHKT1;5-A, the high affinity component of Na^+ transport had a K_m of
139 34 μM ± 26 μM when $[Na^+]_{ext}$ was below 0.1 mM ($K_{m\,(<0.1\,Na)}$), whereas at

140 concentrations of Na^+ above 0.1 mM the K_m was 1.04 ± 0.17 mM ($K_{m\ (> 0.1\ Na)}$) (Fig.
141 4A). The K_m for the higher affinity component of inward Na^+ transport for
142 TaHKT1;5-D was 29 μM ± 4 μM when $[Na^+]_{ext}$ was lower than 0.5 mM ($K_{m\ (< 0.5\ Na)}$),
143 whilst the lower affinity phase had a K_m of 4.32 ± 0.5 mM when $[Na^+]_{ext}$ was higher
144 than 0.5 mM ($K_{m\ (> 0.5\ Na)}$) (Fig. 4B).
145
146 We examined the extent of K^+-inhibition of both the lower and higher affinity
147 components of the inward Na^+ currents when $[K^+]_{ext}$ was 10 mM. The (normalised)
148 inward Na^+ current catalysed by both proteins was significantly suppressed by 10 mM
149 $[K^+]_{ext}$, resulting in negligible inward Na^+ transport by TmHKT1;5-A in presence of
150 $[Na^+]_{ext}$ below 0.1 mM, or by TaHKT1;5-D in presence of $[Na^+]_{ext}$ below 0.5 mM
151 (Fig. 4C and D). In the presence of 10 mM $[K^+]_{ext}$ it was now possible to fit the
152 concentration dependence of inward current through TmHKT1;5-A and TaHKT1;5-D
153 with one component. The K_m of both TmHKT1;5-A and TaHKT1;5-D were decreased
154 approximately by 3-fold by 10 mM $[K^+]_{ext}$ (Fig. 4E and F).
155
156 **Structural modelling of TaHKT1;5-D**
157 Three-dimensional structural models of TaHKT1;5-D were generated to explore why
158 K^+ does not traverse the pore but instead blocks the Na^+ currents, using the KtrB K^+
159 transporter from *B. subtilis* as a template (Vieira-Pires *et al.*, 2013; Xu *et al.*, 2018).
160 The KtrB K^+ protein was crystallised in the presence of KCl, hence the original
161 structure contained a K^+ ion in the selectivity filter region. This ion was substituted by
162 Na^+ during modelling of TaHKT1;5-D as it transports Na^+ but not K^+ (Xu *et el.*,
163 2018). Ramachandran analysis indicated that the template and TaHKT1;5-D models
164 generated in complex with Na^+, and K^+ had satisfactory stereo-chemical quality;
165 Ramachandran plots showed only two residues positioned in disallowed regions
166 (0.5% of all residues, except G and P residues). Average G-factors (measures of
167 correctness of dihedral angles and main-chain covalent forces of protein molecules)
168 calculated by PROCHECK of the template and TaHKT1;5-D models with K^+ and Na^+
169 were 0.06. -0.18 and -0.13, respectively. The ProSa 2003 analysis of z-scores (-8.4; -
170 6.0 and -5.8) indicated that template and modelled structures with K^+ and Na^+ had
171 acceptable conformational energies.
172
173 The TaHKT1;5-D model showed that the Na^+ ion is penta-hedrally coordinated with

174 V76, S77, S78, N231, C232 and H351 (all carbonyl oxygens), that lie near the
175 selectivity filter residues S78, G233, G353 and G457 (Fig. 5A). Notably, the carbonyl
176 oxygen one of the selectivity filter residues (S78) directly participates in Na^+ binding
177 (Fig. 5A). Conversely, the K^+ ion is hexa-hedrally coordinated with V76, N231,
178 C232, H351, N455 and V456, that also closely neighbour the selectivity filter residues
179 (Fig. 5B); here none of the selectivity filter residues participate in direct binding of
180 K^+. The ionic distances of residues neighbouring Na^+ and K^+ ions are within similar
181 ranges: for Na^+ they are between 2.3 and 2.4 Å; for K^+ they are between 2.6 and 2.9 Å
182 (Fig. 5, right panels).
183
184 **Discussion**
185 Oocytes expressing *TmHKT1;5-A* or *TaHKT1;5-D* have been previous reported to
186 undergo no obvious change in their reversal potential regardless of the presence or
187 absence of K^+ in bath solution. Interestingly, both transporters had differential
188 sensitivity to external $[K^+]_{ext}$. Whilst K^+ block occurs for TmHKT1;5-A catalysing
189 inward transport it was not evident at $[Na^+]_{ext}$ above 10 mM, whereas this blockage
190 did happen for TaHKT1;5-D up to 30 mM $[Na^+]_{ext}$ (Fig. 2) (Munns *et al.* 2012; Byrt
191 *et al.* 2014). This differential inhibition effect of K^+ upon Na^+ transport at high
192 $[Na^+]_{ext}$ by TaHKT1;5-D may result from a range of factors, that govern the rates of
193 Na^+ and K^+ ion binding and subsequent Na^+ transport. A variety of factors could
194 control the transport of Na^+ and preliminary displacement of competing K^+ with a
195 consequent energetic cost, before Na^+ passes bare or less-well hydrated than
196 competing K^+. Examples include free-energy variations between ions in binding sites
197 relative to the corresponding quantity in bulk water, differences in selectivity filters
198 solvent exposures (or dielectric constants), overall pore rigidity/stiffness (Dudev and
199 Lim 2010), structural changes within funnels and selectivity filters due to residue re-
200 orientation, differences in the hydration (coordination) numbers of Na^+ and K^+ (Na^+
201 and K^+ bind six and seven water molecules, respectively (Rowley and Roux 2012)
202 and the alterations on the rates of Na^+ or K^+ de-solvation (Degrève *et al.* 1996). It is
203 therefore plausible to expect that both ions would compete for binding sites within
204 HKT funnel regions, yielding ion-protein binding sites with differential binding
205 strengths.
206

207 Here, we refine the previous structural models of HKT1;5 to show that they contain a
208 pore that allows the passage of Na^+ but not K^+ (Cotsaftis *et al.*, 2012; Waters *et al.*,
209 2013; Xu *et al.*, 2018). This is consistent with the functional observations in this and
210 previous studies (Munns *et al.* 2012; Byrt *et al.* 2014). Previously it was suggested
211 that the Gly-Gly-Gly-Gly motif is important in coordinating the K^+ ion in Ktr/TrK
212 transporters and in conferring dual Na^+-K^+ transport in HKT2 transporters (Durrell
213 and Guy, 1999; Mäser *et al.* 2002). Here our modelling suggests that the serine residue
214 within the Ser-Gly-Gly-Gly selectivity motif directly interacts and binds with Na^+ (Fig
215 5B). Furthermore, our model suggests, despite ionic distances being shorter for Na^+
216 than those for K^+, that K^+ could be bound more strongly due to a higher coordination
217 pattern (Fig. 5A and 5B-right panels). Obviously, during binding, K^+ takes an
218 advantage of its larger ionic radius: 152 picometer (pm), compared to that of Na^+ (116
219 pm); these parameters reflects empirical atomic radii of K (220 pm) and Na (180 pm).
220 We assume that under the high concentrations of K^+, this ion may outcompete Na^+ and
221 would become bound in the selectivity filter, thus effectively blocking Na^+ transport.
222 This is illustrated by calculating permeation channels in both complexes, using the
223 Mole Voronoi algorithm, that predicts permeation trajectories and identifies path
224 bottlenecks. From the calculated permeation paths, it could be deduced that the K^+ ion
225 effectively blocks the permeation channel through the major gating protein pore,
226 contrary to Na^+. It is also obvious that Na^+ is likely to enter and exit the permeation
227 trajectory from several points on both sides of the transporter, but always by-passes
228 the selectivity filter constriction. Both ions arrive at the funnel of HKT proteins in
229 solvated (hydrated) forms. While the hydration number for Na^+ is 6, that for K^+ is 7 at
230 ambient temperature (Rowley and Roux 2012; Ma, 2016). The significance of the
231 seven-fold water coordination for K^+ is that this solvated complex may form a
232 stronger hydrogen-bond interaction pattern (in funnels of HKT proteins), and would
233 be de-solvated with a higher energy input and thus slower) that the Na^+ solvated
234 complex (Degrève et al., 1996). It is also plausible to expect that both solvated ion
235 complexes would compete for binding sites within HKT funnel regions with different
236 binding strengths. All in all, this would contribute to the blockage of the pore entry of
237 HKT transporters.
238
239 Potassium permeability for HKT1 transporters has only been reported once for the
240 proteins that have been characterised in *X. laevis* oocytes. The transporters EcHKT1;1

241 and EcHKT1;2 allow permeation of both K^+ and Na^+ (Liu *et al.*, 2001). Interestingly,
242 when 3D models of the Na^+ selective OsHKT1;5 and K^+ permeable EcHKT1;2 were
243 constructed and compared the pore size was predicted to be 0.2 Å larger in EcHKT1;2
244 (than OsHKT1;5 and TaHKT1;5-D), which would more than account for the weaker
245 interactions with K^+ and allow this larger ion to pass through the pore (Waters *et al.*,
246 2013). Without 3D modelling of each and every transporter in the HKT family to
247 show how the selectivity filter forms in the context of the rest of the protein it would
248 not be possible to predict which other HKT1s may allow passage of K^+. Predictions
249 based on sequence alone are insufficient to predict how the two sets of proteins
250 evolved their individual Na^+ and K^+ transport characteristics. An extension of the
251 model to include other HKT proteins, a greater survey of structure-function
252 relationships and mutations of key residues to predict functionally relevant residues
253 and evolutionary relationships will be the focus of further study.
254
255 Two affinity ranges for Na^+ transport have been detected in the HKT family
256 previously, but only for HKT2 transporters. OsHKT2;1, OsHKT2;2, OsHKT2;4 and
257 HvHKT2;1(Schachtman and Schroeder 1994; Rubio *et al.* 1995; Jabnoune *et al.* 2009;
258 Yao *et al.* 2010; Horie *et al.* 2011; Sassi *et al.* 2012). For instance, for OsHKT2;2,
259 when K^+ is present, the transport of Na^+ is K^+-dependent and displays a high affinity
260 (K_m = 0.077 mM), whereas showing a lower affinity when absence of K^+ (K_m= 16
261 mM) (Rubio *et al.* 1995; Yao *et al.* 2010). OsHKT2;1 also acquires two phases of
262 Na^+-transport affinity, whose K_m for Na^+ is respectively 9.5 µM at $[Na^+]_{ext}$ below 1
263 mM and is 2.2 mM at $[Na^+]_{ext}$ > 1 mM (Jabnoune *et al.* 2009). The K^+ transport
264 catalysed by HvHKT2;1 is affected by both $[Na^+]_{ext}$ and $[K^+]_{ext}$, such as a decrease in
265 its K^+ transport affinity from 30 µM down to 3.5 mM by $[Na^+]_{ext}$ increased from 0.5
266 mM to 30 mM and a greatly reduced channel conductivity for K^+ by increasing $[K^+]_{ext}$
267 above ~3 mM (Mian *et al.* 2011). This is the first time that dual affinity characteristics
268 have been reported for the HKT1;*x* family (Fig. 4). Considering the considerably
269 homology between both clades (58% similarity/41% identity between TaHKT1;5 and
270 TaHKT2;1) it is perhaps not surprising that both clades can confer dual affinity
271 transport. How such ability is conferred structurally is still to be determined.
272
273 In summary, whilst the high-affinity component was similarly inhibited by 10 mM
274 $[K^+]_{ext}$ for both TaHKT1;5-D and TmHKT1;5-A, the low affinity component of Na^+

275 transport for TmHKT1;5-A was less inhibited by external K than TaHKT1;5-D (Fig.
276 4). Furthermore, both wheat HKT1;5 proteins facilitate Na^+ uptake at high affinity;
277 TmHKT1;5-A facilitates Na^+ uptake with a higher affinity than TaHKT1;5-D
278 regardless the absence or presence of $[K^+]_{ext,}$ (Fig. 4) (Munns *et al.* 2012; Byrt *et al.*
279 2014). TmHKT1;5-A has been shown to be more effective in conferring shoot Na^+
280 exclusion to wheat compared to TaHKT1;5-D (James *et al.*, 2012). We propose that
281 the higher affinity (with half-maximal activity nearer 1 mM compared to 4 mM), and
282 a lower sensitivity to $[K^+]_{ext}$ are both characteristics that can help confer better shoot
283 Na^+ exclusion, which is a property that can lead to greater salt tolerance in the field
284 for wheat (James *et al.* 2011; James *et al.* 2012; Munns *et al.* 2012).
285
286 **Materials and Methods**
287 Brief methods for cloning of *TmHKT1;5-A* and *TaHKT1;5-D* as well as its functional
288 characterisation in heterologous expression systems were described Munns et al.
289 (Munns *et al.* 2012) and Byrt et al. (Byrt *et al.* 2014). Further details are included
290 here.
291
292 **Two-electrode voltage clamp recording in *X. laevis* oocytes**
293 Oocyte recording followed the methods as described in Munns et al. (Munns *et al.*
294 2012)and Byrt et al. (Byrt *et al.* 2014). Briefly, 46 nl/23 ng of cRNA or equal
295 volumes of RNA-free water were injected into oocytes, followed by an incubation for
296 48 h before recording. Membrane currents were recorded in the HMg solution (6 mM
297 $MgCl_2$, 1.8 mM $CaCl_2$, 10 mM MES and pH 6.5 adjusted with a TRIS base) ± Na^+
298 glutamate and/or K^+ glutamate as indicated. All solution osmolarities were adjusted
299 using mannitol at 220-240 mOsmol kg^{-1}.
300
301 **Construction of 3D models of TaHKT1;5D in complex with Na^+ and K^+ ions**
302 The most suitable template for TaHKT1;5D, the KtrB K^+ transporter from *B. subtilis*
303 (Protein Data Bank accession 4J7C, chain I) (Vieira-Pires et al., 2013), was identified
304 as previously described (Xu et al., 2017). The KtrB K^+ protein was crystallised in the
305 presence of KCl, hence the structure contains a K^+ ion in the selectivity filter region.
306 This ion was substituted by Na^+ during modelling of TaHKT1;5D that transport Na^+ at
307 a greater rate than K^+ (Xu et el., 2017). 3D structural models in complex with Na^+, and
308 K^+ were generated using Modeller 9v16 (Sali and Blundell, 1993) on a Linux station

309 running the Fedora 12 operating system, as previously described (Cotsaftis et al.,
310 2012, Waters et al., 2013, Xu et al., 2017). During modelling, attention was paid to
311 ionic radii of Na^+, and K^+, whose topology parameters were taken from CHARMM
312 (Brooks et al., 2009). In each case, a total of 100 models were generated that were
313 scored by Modeller using the modeller objective function (Shen and Sali, 2006), the
314 discrete optimised protein energy function (Eswar et al., 2008), PROCHECK
315 (Laskowski et al., 1993), ProSa 2003 (Sippl, 1993) and FoldX (Schymkowitz et al.,
316 2005). Best scoring models constructed in Modeller 9v19 were further subjected to
317 energy minimisation (knowledge-based Yasara2 forcefield with parameters for bond
318 distances, planarity of peptide bonds, bond angles, Coulomb terms, dihedral angles,
319 and van der Waals forces) (Krieger et al., 2004) combined with the particle-mesh-
320 Ewald (PME) energy function for long range electrostatics (cutoff 8.0 Å), to obtain
321 smoothed electrostatic potentials. Structural images were generated with PyMOL
322 Molecular Graphics System V1.8.2.0 (Schrődinger LLC, Portland, OR, USA).
323
324 **Funding**
325 This work was supported by funding to M.G. from the Grains Research and
326 Development Corporation (UA00145, M.G.), and Australian Research Council
327 through the Centre of Excellence (CE1400008) and Future Fellowship
328 (FT130100709) schemes.
329
330

331 **References**

332 Almeida, P, de Boer, G-J, de Boer, AH (2014a) Differences in shoot Na^+
333 accumulation between two tomato species are due to differences in ion affinity
334 of HKT1;2. *Journal of Plant Physiology* **171**, 438-447.
335 Almeida, P, Feron, R, de Boer, G-J, de Boer, AH (2014b) Role of Na^+, K^+, Cl^-,
336 proline and sucrose concentrations in determining salinity tolerance and their
337 correlation with the expression of multiple genes in tomato. *AoB Plants* **6**,
338 plu039.
339 Asins, MJ, Villalta, I, Aly, MM, Olias, R, Álvarez De Morales, P, Huertas, R, Li, J,
340 JAIME-PÉREZ, N, Haro, R, Raga, V (2013) Two closely linked tomato HKT
341 coding genes are positional candidates for the major tomato QTL involved in
342 Na^+/K^+ homeostasis. *Plant, Cell & Environment* **36**, 1171-1191.
343 Ben Amar, S, Brini, F, Sentenac, H, Masmoudi, K, Véry, A-A (2013) Functional
344 characterization in Xenopus oocytes of Na^+ transport systems from durum
345 wheat reveals diversity among two HKT1; 4 transporters. *Journal of*
346 *experimental botany* **65**, 213-222.
347 Byrt, CS, Xu, B, Krishnan, M, Lightfoot, DJ, Athman, A, Jacobs, AK, Watson-Haigh,
348 NS, Plett, D, Munns, R, Tester, M (2014) The Na^+ transporter, TaHKT1;5-D,
349 limits shoot Na^+ accumulation in bread wheat. *Plant Journal* **80**, 516-526.
350 Campbell, MT, Bandillo, N, Al Shiblawi, FRA, Sharma, S, Liu, K, Du, Q, Schmitz,
351 AJ, Zhang, C, Véry, A-A, Lorenz, AJ (2017) Allelic variants of OsHKT1; 1
352 underlie the divergence between indica and japonica subspecies of rice (*Oryza*
353 *sativa*) for root sodium content. *PLoS genetics* **13**, e1006823.
354 Corratgé-Faillie, C, Jabnoune, M, Zimmermann, S, Véry, A-A, Fizames, C, Sentenac,
355 H (2010) Potassium and sodium transport in non-animal cells: the
356 Trk/Ktr/HKT transporter family. *Cellular and Molecular Life Sciences* **67**,
357 2511-2532.
358 Cotsaftis, O, Plett, D, Shirley, N, Tester, M, Hrmova, M (2012) A two-staged model
359 of Na^+ exclusion in rice explained by 3D modeling of HKT transporters and
360 alternative splicing. *PLoS One* **7**, e39865.
361 Degrève, L, Vechi, SM, Junior, CQ (1996) The hydration structure of the Na^+ and K^+
362 ions and the selectivity of their ionic channels. *Biochimica et Biophysica Acta*
363 *(BBA)-Bioenergetics* **1274**, 149-156.
364 Dudev, T, Lim, C (2010) Factors governing the Na^+ vs K^+ selectivity in sodium ion
365 channels. *Journal of the American Chemical Society* **132**, 2321-2332.
366 Henderson SW, Dunlevy JD, Wu Y, Blackmore DH, Walker RR, Edwards EJ,
367 Gilliham M, Walker AR (2018) Functional differences in transport properties
368 of natural HKT1;1 variants influence shoot Na^+ exclusion in grapevine
369 rootstocks. *New Phytologist* **217**, 113-1127.
370 Horie, T, Brodsky, DE, Costa, A, Kaneko, T, Schiavo, FL, Katsuhara, M, Schroeder,
371 JI (2011) K^+ transport by the OsHKT2; 4 transporter from rice with atypical
372 Na^+ transport properties and competition in permeation of K^+ over Mg^{2+} and
373 Ca^{2+} ions. *Plant Physiology* **156**, 1493-1507.
374 Jabnoune, M, Espeout, S, Mieulet, D, Fizames, C, Verdeil, J-L, Conéjéro, G,
375 Rodríguez-Navarro, A, Sentenac, H, Guiderdoni, E, Abdelly, C (2009)
376 Diversity in expression patterns and functional properties in the rice HKT
377 transporter family. *Plant Physiology* **150**, 1955-1971.
378 James, RA, Blake, C, Byrt, CS, Munns, R (2011) Major genes for Na^+ exclusion,
379 *Nax1* and *Nax2* (wheat *HKT1; 4* and *HKT1; 5*), decrease Na+ accumulation in

380 bread wheat leaves under saline and waterlogged conditions. *Journal of*
381 *experimental botany* **62**, 2939-2947.
382 James, RA, Blake, C, Zwart, AB, Hare, RA, Rathjen, AJ, Munns, R (2012) Impact of
383 ancestral wheat sodium exclusion genes *Nax1* and *Nax2* on grain yield of
384 durum wheat on saline soils. *Functional Plant Biology* **39**, 609-618.
385 James, RA, Davenport, RJ, Munns, R (2006) Physiological characterization of two
386 genes for Na^+ exclusion in durum wheat, *Nax1* and *Nax2*. *Plant Physiology*
387 **142**, 1537-1547.
388 Lan, W-Z, Wang, W, Wang, S-M, Li, L-G, Buchanan, BB, Lin, H-X, Gao, J-P, Luan,
389 S (2010) A rice high-affinity potassium transporter (HKT) conceals a calcium-
390 permeable cation channel. *Proceedings of the National Academy of Sciences,*
391 *U.S.A.* **107**, 7089-7094.
392 Liu, W, Fairbairn, DJ, Reid, RJ, Schachtman, DP (2001) Characterization of two
393 HKT1 homologues from *Eucalyptus camaldulensis* that display intrinsic
394 osmosensing capability. *Plant Physiol.* **127**, 283-294.
395 Mäser, P, Hosoo, Y, Goshima, S, Horie, T, Eckelman, B, Yamada, K, Yoshida, K,
396 Bakker, EP, Shinmyo, A, Oiki, S (2002) Glycine residues in potassium
397 channel-like selectivity filters determine potassium selectivity in four-loop-
398 per-subunit HKT transporters from plants. *Proceedings of the National*
399 *Academy of Sciences, U.S.A.* **99**, 6428-6433.
400 Mian, A, Oomen, RJ, Isayenkov, S, Sentenac, H, Maathuis, FJ, Véry, AA (2011)
401 Over-expression of an Na^+-and K^+-permeable HKT transporter in barley
402 improves salt tolerance. *Plant Journal* **68**, 468-479.
403 Munns, R, James, RA, Xu, B, Athman, A, Conn, SJ, Jordans, C, Byrt, CS, Hare, RA,
404 Tyerman, SD, Tester, M, Plett, D, Gilliham, M (2012) Wheat grain yield on
405 saline soils is improved by an ancestral Na^+ transporter gene. *Nature*
406 *Biotechnology* **30**, 360-364.
407 Munns, R, Gilliham, M (2015) Salinity tolerance of crops - What is the cost? *New*
408 *Phytologist* **208**, 668-673.
409 Platten, JD, Cotsaftis, O, Berthomieu, P, Bohnert, H, Davenport, RJ, Fairbairn, DJ,
410 Horie, T, Leigh, RA, Lin, H-X, Luan, S (2006) Nomenclature for HKT
411 transporters, key determinants of plant salinity tolerance. *Trends in Plant*
412 *Sciences* **11**, 372-374.
413 Ren, Z-H, Gao, J-P, Li, L-G, Cai, X-L, Huang, W, Chao, D-Y, Zhu, M-Z, Wang, Z-Y,
414 Luan, S, Lin, H-X (2005) A rice quantitative trait locus for salt tolerance
415 encodes a sodium transporter. *Nature Genetics* **37**, 1141-1146.
416 Rowley, CN, Roux, Bt (2012) The solvation structure of Na^+ and K^+ in liquid water
417 determined from high level ab initio molecular dynamics simulations. *Journal*
418 *of chemical theory and computation* **8**, 3526-3535.
419 Rubio, F, Gassmann, W, Schroeder, JI (1995) Sodium-driven potassium uptake by the
420 plant potassium transporter HKT1 and mutations conferring salt tolerance.
421 *Science* **270**, 1660.
422 Sassi, A, Mieulet, D, Khan, I, Moreau, B, Gaillard, I, Sentenac, H, Véry, A-A (2012)
423 The rice monovalent cation transporter OsHKT2; 4: revisited ionic selectivity.
424 *Plant Physiology* **160**, 498-510.
425 Schachtman, DP, Schroeder, JI (1994) Structure and transport mechanism of a high-
426 affinity potassium uptake transporter from higher plants. *Nature* **370**, 655-658.
427 Sentenac, H, Bonneaud, N (1992) Cloning and expression in yeast of a plant
428 potassium ion transport system. *Science* **256**, 663.

429 Uozumi, N, Kim, EJ, Rubio, F, Yamaguchi, T, Muto, S, Tsuboi, A, Bakker, EP,
430 Nakamura, T, Schroeder, JI (2000) The Arabidopsis HKT1 gene homolog
431 mediates inward Na^+ currents in *Xenopus laevis* oocytes and Na^+ uptake in
432 *Saccharomyces cerevisiae*. *Plant Physiology* **122**, 1249-1260.
433 Waters, S, Gilliham, M, Hrmova, M (2013) Plant high-affinity potassium (HKT)
434 transporters involved in salinity tolerance: structural insights to probe
435 differences in ion selectivity. *International Journal of Molecular Sciences* **14**,
436 7660-7680.
437 Xu, B, Waters, S, Byrt, CS, Plett, D, Tyerman, SD, Tester, M, Munns, R, Hrmova, M,
438 Gilliham, M (2018) Structural variations in wheat HKT1; 5 underpin
439 differences in Na^+ transport capacity. *Cellular and Molecular Life Sciences* 1-
440 12.
441 Yao, X, Horie, T, Xue, S, Leung, H-Y, Katsuhara, M, Brodsky, DE, Wu, Y,
442 Schroeder, JI (2010) Differential sodium and potassium transport selectivities
443 of the rice OsHKT2; 1 and OsHKT2; 2 transporters in plant cells. *Plant*
444 *Physiology* **152**, 341-355.
445

446

447 **Figures**

448 **Figure 1. K^+-sensitivity of Na^+ currents carried by TmHKT1;5-A and**
449 **TaHKT1;5-D.** A-D, current-voltage (I/V) curves of Na^+ currents recorded from *X.*
450 *laevis* oocytes expressing *TmHKT1*;5-*A* (A, C) and *TaHKT1*;5-*D* (B, D) in 1 mM Na^+
451 plus 0-30 mM K^+ (A,B), or 0-30 mM Na^+ solutions with or without 10 mM K^+ (C,D).
452 Mean ± S.E.M, n = 5-6.
453

454 **Figure 2. Channel conductance of TmHKT1;5-A and TaHKT1;5-D.** The channel
455 conductance of TmHKT1;5-A and TaHKT1;5-D was calculated from Figure 1, based
456 on the slope of curve between -140 mV and -120 mV, statistical difference was
457 determined by *Students' t-test*, $*P < 0.05$ and $** P < 0.01$.
458

459 **Figure 3. Shift in reversal potential of TmHKT1;5-A and TaHKT1;5-D in**
460 **response to changes in $[Na^+]_{ext}$ and $[K^+]_{ext}$.**
461 A, Reversal potential of currents in *X. laevis* oocytes expressing *TmHKT1*;5-*A* and
462 *TaHKT1*;5-*D* derived from Figure. 1. B, Reversal potential of Na^+ currents plotted
463 against theoretical Nernst potential derived from internal concentrations measured in
464 Munns et al. (2012) and Byrt et al., (2014) at the used.
465 Nernst shift in oocytes expressing *TmHKT1*;5-*A* and *TaHKT1*;5-*D* from 1 mM to 10
466 mM Na^+ ($[1\text{-}10]_{ext}$ Na^+) and 10 mM to 30 mM Na^+ ($[10\text{-}30]_{ext}$ Na^+) with or without 10
467 mM $[K^+]_{ext}$, $\Delta Exp._{Na}$ = experimentally measured shift in reversal potential for Na^+, the
468 theortectical equilibrium (or Nernst) potential for Na^+ was 57.7 mV and 26.9 mV,
469 respectively for $[1\text{-}10]_{ext}$ Na^+ and $[10\text{-}30]_{ext}$ Na^+, refers to Munns et al. (2012).
470

471 **Figure 4. Transport affinity of TmHKT1;5-A and TaHKT1;5-D in *X. laevis***
472 **oocytes.**
473 A-B, dual Na^+-transport affinity of TmHKT1;5-A and TaHKT1;5-D in *X. laevis*
474 oocytes, plotted as normalised currents at -140 mV as shown against a series of Na^+
475 glutamate solutions. C-D, high affinity phase of TmHKT1;5-A and TaHKT1;5-D in
476 absence and presence of 10 mM $[K^+]_{ext}$. Data represented in A, B and C as mean ±
477 S.E.M (n = 5 for A, n = 4 for B, n = 7 for C). E-F, Na^+-transport affinity of
478 TmHKT1;5-A and TaHKT1;5-D in *X. laevis* oocytes, plotted as normalised currents
479 at -140 mV as shown against a series of Na^+ glutamate solutions with an additional 10
480 mM K^+ glutamate.

481

482 **Figure 5. Molecular models of TaHKT1;5D in complex with Na^+ (A) and K^+ (B)**
483 **ions.**

484 **(A-B; left panels)** Cartoon representations of TaHKT1;5-D illustrate their overall
485 protein folds with cylindrical α-helices, and permeation channels (black mesh). Na^+
486 (A) and K^+ (B) ions are shown as purple spheres located within the selectivity filter
487 residues S78, G233, G353 and G457 (coloured in cpk magenta), and other
488 neighbouring residues. Na^+ is likely to enter and exit the permeation trajectory from
489 several points on both sides of the transporter, but always by-passes the selectivity
490 filter constriction. K^+ enters the selectivity filter and effectively blocks the gating
491 trajectory.

492 **(A-B; right panels)** Detailed views of bound Na^+ and K^+ ions that interact through
493 respective penta-hedral (yellow dashed lines) and hexa-hedral (green dashed lines)
494 coordination patterns with residues adjoining the selectivity filter residues S78, G233,
495 G353 and G457. The ionic distances of 2.3-2.8 Å for Na^+ between V76, S77, S78,
496 N231, C232 and H351, and of 2.6-2.9 Å for K^+ between V76, N231, C232, H351,
497 N455 and V456, are formed between carbonyl oxygens of these residues (in sticks in
498 atomic colours), located near selectivity filter residues. The K^+ ion effectively blocks
499 the permeation channel through the protein pore, contrary to Na^+.
500

501 **Figure 1**

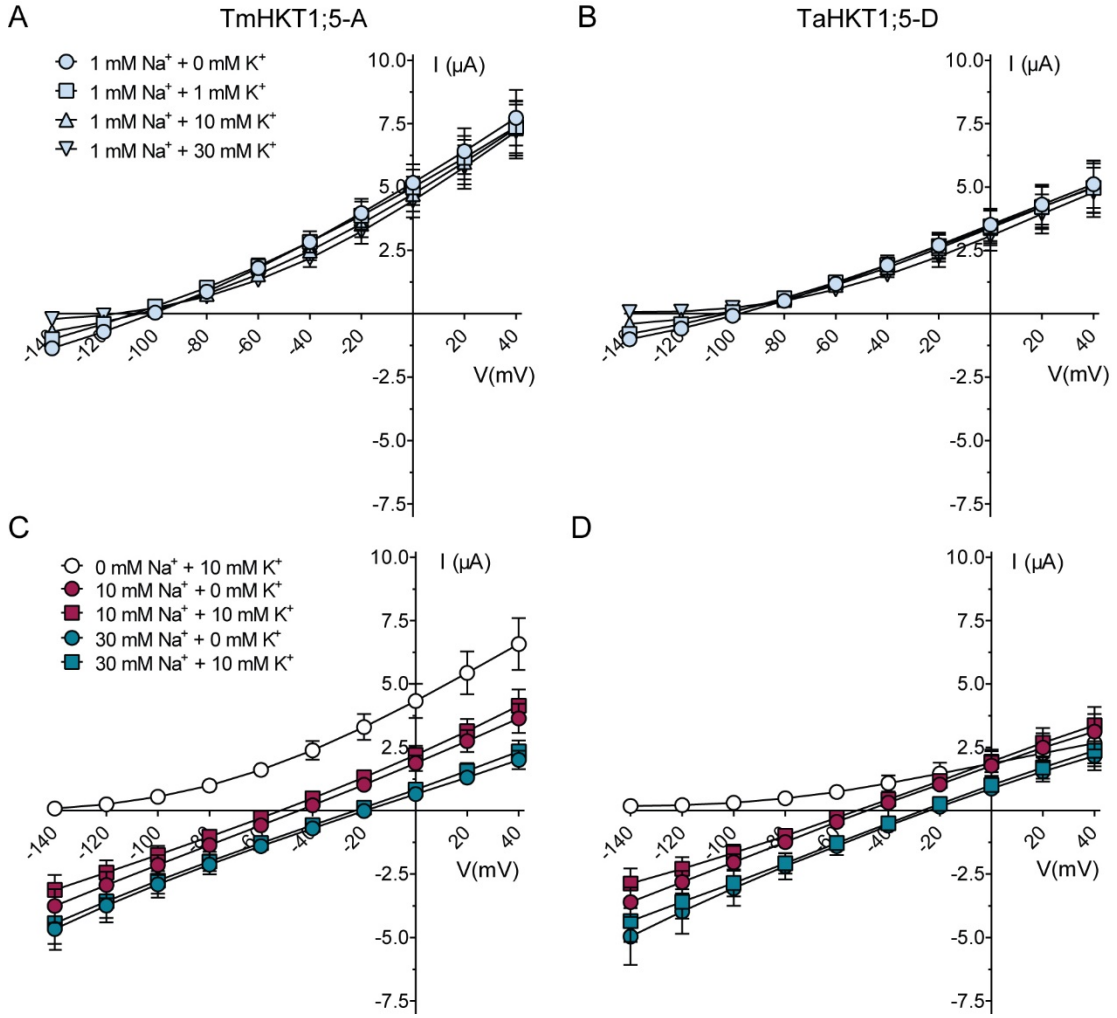

502

503

504

505 **Figure 2**

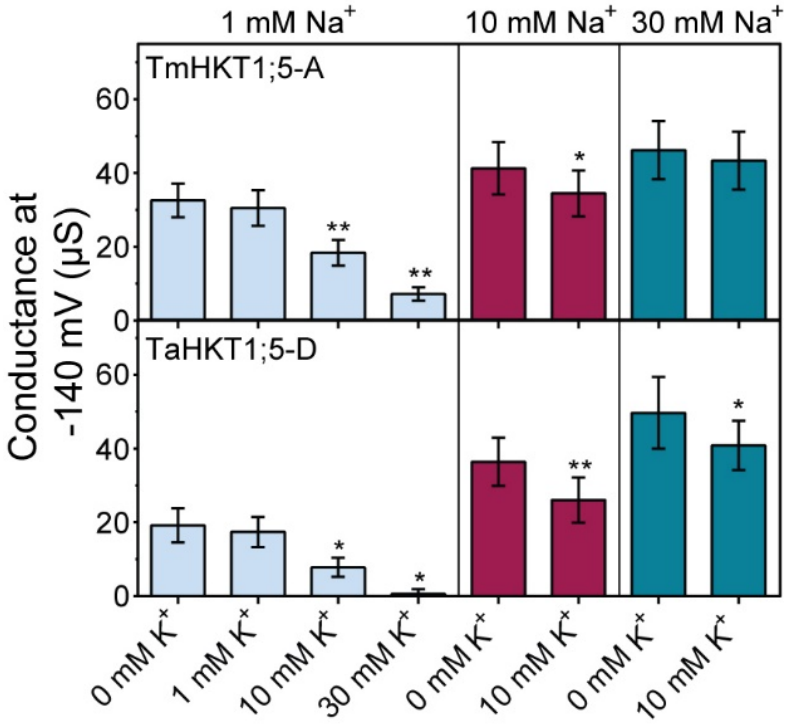

506

507

508 **Figure 3**

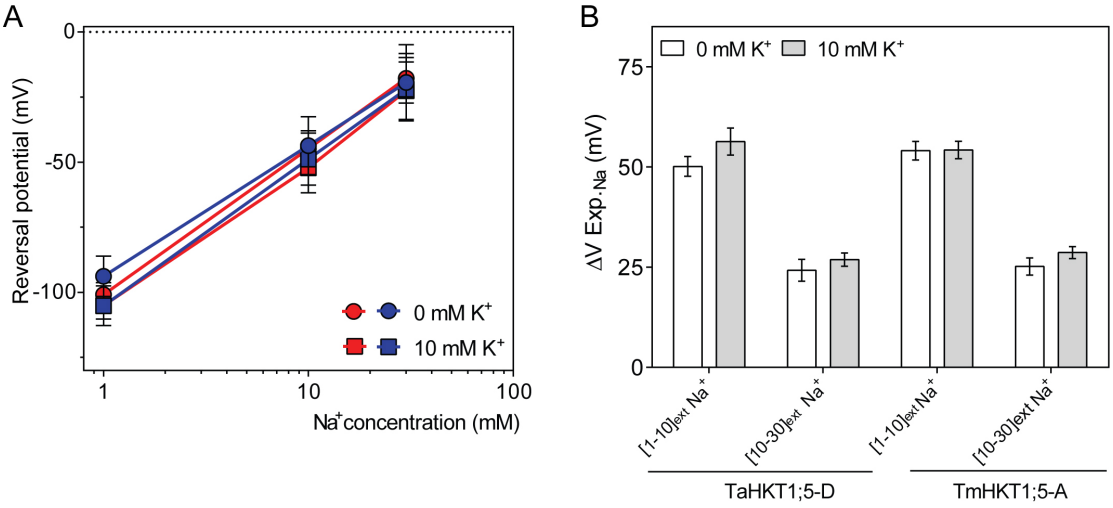

509

510

511 **Figure 4**

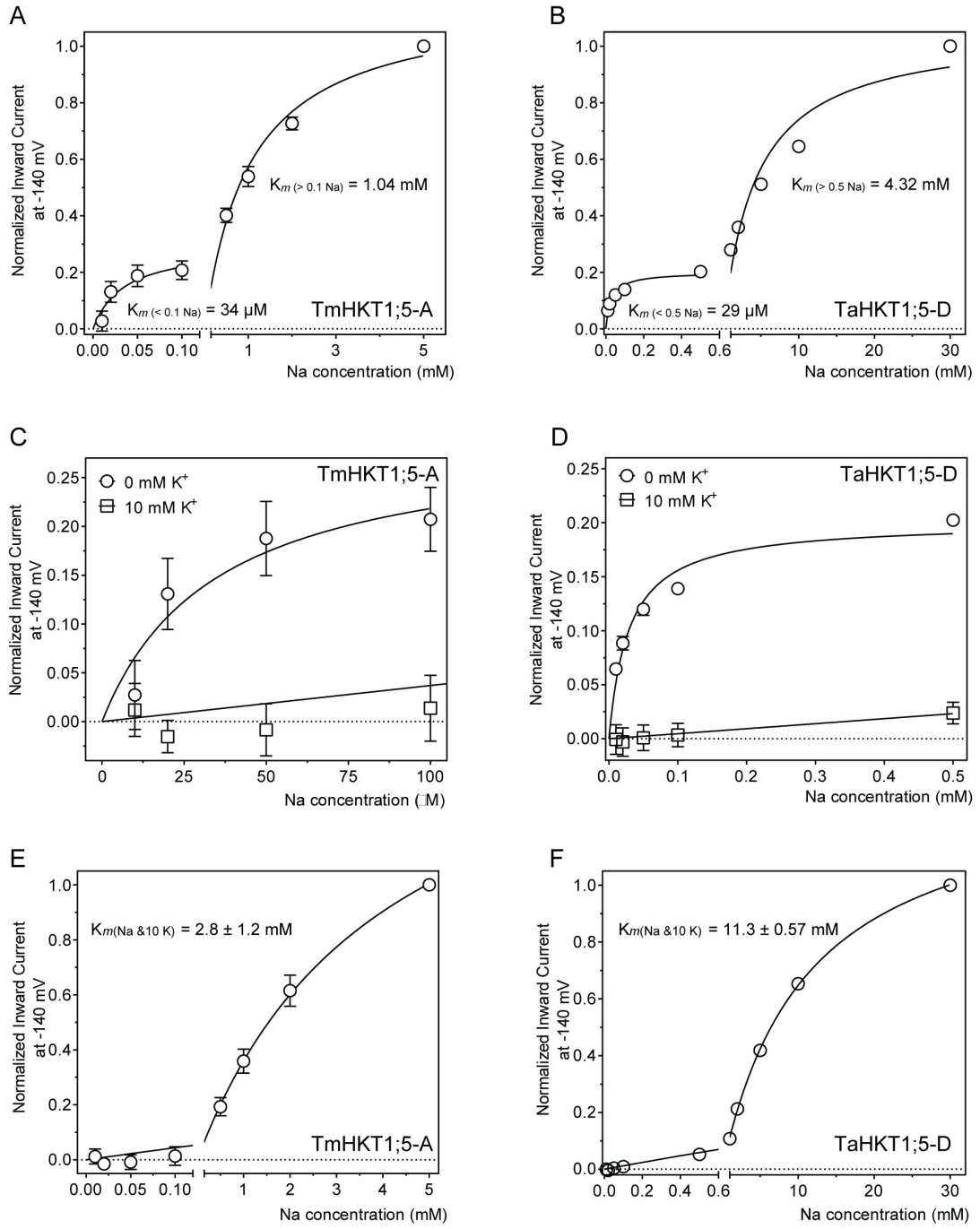

512

513

514

515 **Figure 5**

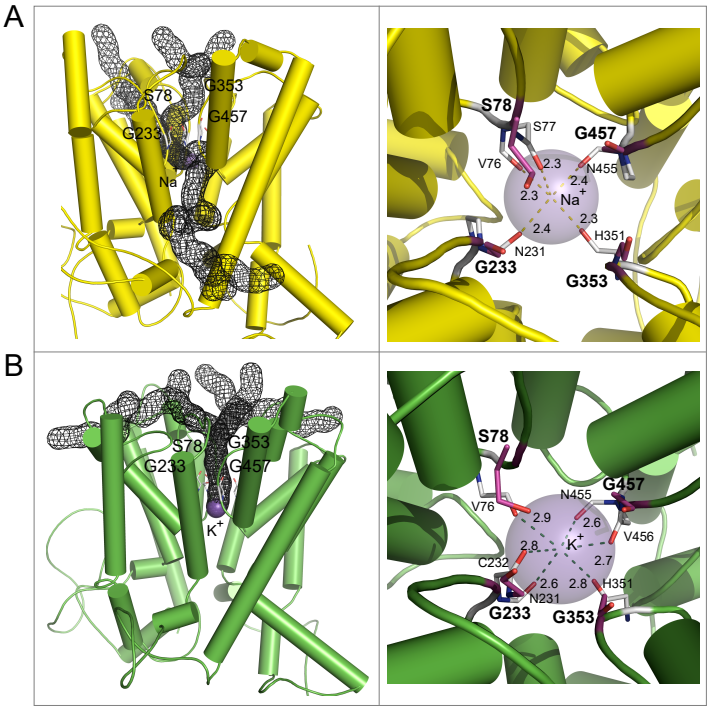

516
517